IOP Publishing Journal of Physics B: Atomic, Molecular and Optical Physics
J. Phys. B: At. Mol. Opt. Phys. **57** (2024) 105002 (8pp) https://doi.org/10.1088/1361-6455/ad38f4

Calculation of forbidden transitions in doubly ionized neodymium (Nd III) of interest for kilonova nebular phase analysis

L Maison[1], **P Palmeri**[1] **and P Quinet**[1,2,*]

[1] Physique Atomique et Astrophysique, Université de Mons—UMONS, B-7000 Mons, Belgium
[2] IPNAS, Université de Liège, B-4000 Liège, Belgium

E-mail: pascal.quinet@umons.ac.be

Received 22 January 2024, revised 6 March 2024
Accepted for publication 28 March 2024
Published 18 April 2024

Abstract

In this paper, we present new radiative rate calculations for forbidden transitions, namely magnetic dipole (M1) and electric quadrupole (E2) transitions, involving all the experimentally known energy levels within the $4f^4$ ground configuration of doubly ionized neodymium (Nd III). To do this, and in order to estimate the accuracy of the results obtained, two independent computational approaches based on the pseudo-relativistic Hartree–Fock and the fully relativistic Dirac-Hartree–Fock methods were used. The transition probabilities calculated with these two approaches showed good overall agreement, in particular for the most intense forbidden lines for which the relative differences did not exceed 25%. From these new atomic data, some astrophysical implications were deduced such as the possibility (or not) of observing some [Nd III] lines on the infrared spectra recorded by the *James Webb Space Telescope*, more precisely for the analysis of nebular phase kilonova spectra following compact object mergers.

Keywords: atomic data, atomic processes, forbidden lines, kilonovae

1. Introduction

Since the detection of a neutron star merger (NSM) in August 2017 from the observation of gravitational waves using the *LIGO* and *VIRGO* instruments, known as the GW170817 event (Abbott *et al* 2017), the radiative properties of heavy elements (heavier than iron) have sparked renewed interest. These elements are in fact produced in large quantities during coalescence from the nucleosynthesis r-process and their presence has been detected in the electromagnetic signal, called AT2017gfo kilonova, recorded by numerous telescopes in the infrared, visible, ultraviolet and x-ray domains (Kasen *et al* 2017, Pian *et al* 2017, Smartt *et al* 2017, Siegel 2022, Pian 2023).

In the first days after the merger, the kilonova spectrum is essentially characterized by a multitude of absorption lines caused by millions of allowed transitions, i.e. electric dipole transitions (E2), belonging to the different heavy elements present in the ejecta, leading to a significant opacity in the observed spectrum (see e.g. Kasen *et al* 2017). As time passes, the temperature and density of the ejecta decrease leading to a nebular phase of the kilonova whose the infrared spectrum detected by the *Spitzer Space Telescope* was assumed by Kasliwal *et al* (2022) to contain forbidden lines of magnetic (M1) and electric quadrupole (E2) types. These latter authors in fact supposed that forbidden transitions of Se III, Rh III, Ce IV, W III or Os III could contribute to the observed spectral features while pointing out that the lack of accurate atomic data for forbidden lines in heavy elements strongly complicated the modeling of the observed peculiar emission features.

* Author to whom any correspondence should be addressed.

The importance of M1 and E2 transitions in kilonova modeling was notably discussed by Gillanders *et al* (2021) who showed how the inclusion of such transitions in heavy elements can lead to the identification of elemental signatures through radiative transfer calculations. The nebular phase of lanthanide-rich NSM ejecta was simulated by Hotokezaka *et al* (2021) who solved the ionization and thermal balance of the ejecta under non-local thermodynamic equilibrium using a single atomic species, namely neodymium, for which the energy levels, transition probabilities, collision strengths and recombination rates were estimated with GRASP2K (Jönsson *et al* 2013) and HULLAC (Bar-Shalom *et al* 2001) atomic structure codes. In that work, it was found that both allowed and forbidden lines almost equally contribute to the cooling rate of Nd II and Nd III at nebular temperatures.

Very recently, Gillanders *et al* (2023) reported *James Webb Space Telescope* (*JWST*) spectroscopic observations of a rapidly-reddening thermal transient, following the gamma-ray burst, GRB 23 0307A, produced by the merger of compact objects. In particular, at $T_0 + 29$ days, i.e. 29 days after merger, the *JWST* emission spectrum showed two features at $\sim$2.1 μm and $\sim$4.4 μm for which Gillanders *et al* (2023) established a shortlist of candidate forbidden transitions that could contribute to the observed spectral profiles. Among those transitions, the same [Te III] line as the one proposed by Levan *et al* (2023) was recovered and supplemented with M1 and (E2) lines of various heavy ions, among which a handful belonging to lanthanide ions, such as neodymium and erbium. It was nevertheless emphasized by Gillanders *et al* (2023) that further investigations of these species, with the aim of providing reliable transition rates for forbidden lines, were necessary to confirm the contribution of any of these lines to the kilonova emission spectra. In this context, lanthanide elements are of particular importance since they are among the most abundant elements in the material ejected after the merger of compact objects.

Concerning forbidden transitions in neutral, singly- and doubly-ionized lanthanides, previously published works were dedicated to La II (Derkatch *et al* 2002, Rostohar *et al* 2003, Li *et al* 2014), La III (Roberts *et al* 2013, Safronova and Safronova 2014), Ce III (Li *et al* 2014), Pr III (Li *et al* 2016), Nd II (Biémont *et al* 2007), Sm I (Beck and O'Malley 2010), Eu II (Rostohar *et al* 2001), Tm I (Kolachevsky *et al* 2007, Sukachev *et al* 2016), Yb I (Migdalek and Baylis 1991, Bowers *et al* 1999, Mishra and Balasubramanian 2001, Stalnaker *et al* 2002, Beloy *et al* 2007, Tsigutkin *et al* 2009, 2010, Dzuba and Derevianko 2010, Karaçoban and Özdemir 2011, Nandy and Sahoo 2014, Xu *et al* 2014, Roberts *et al* 2014a, 2015, Dzuba *et al* 2018, Safronova *et al* 2018, Kozlov *et al* 2019), Yb II (Gerz *et al* 1988, Fawcett and Wilson 1991, Roberts *et al* 1997, 2014b, Biémont and Quinet 1998, Yu and Maleki 2000, Dzuba and Flambaun 2011, 2012, Sahoo and Das 2011, Chaudhuri *et al* 2012, Gossel *et al* 2013, Lange *et al* 2021, Tan *et al* 2021), Yb III (Safronova and Safronova 2009, Allehabi *et al* 2021), Lu II (Arnold *et al* 2016, Paez *et al* 2016) and Lu III (Safronova *et al* 2016). Looking in more detail at this list of previous investigations, we note that some lanthanide ions have no data available for forbidden transitions. This is particularly the case of Nd III for which we have chosen to focus the present study. This ion is characterized by the $4f^4$ ground configuration for which 16 energy levels were recently experimentally determined from the neodymium spectra emitted by Penning and hollow cathode discharge lamps and analyzed using high resolving power Fourier transform spectroscopy (Ding *et al* 2023).

The main goal of the present work is to provide new radiative rates for forbidden transitions, i.e. magnetic dipole (M1) and electric quadrupole (E2) transitions, involving all the 16 experimentally known levels within the $4f^4$ ground configuration of Nd III. To do this, two independent computational methods were used, namely the pseudo-relativistic Hartree–Fock (HFR) and the fully relativistic multiconfiguration Dirac-Hartree–Fock (MCDHF) approaches. These calculations allowed us to highlight the most intense Nd III forbidden lines likely to be observed in astrophysical spectra emitted from low density environments such as the nebular phase of kilonovae for example.

2. Computational approaches

2.1. HFR calculations

In a first step, we used the HFR method developed by Cowan (1981) for computing the transition rates of forbidden lines in Nd III. The physical model used in these calculations was based on the model considered in our previous study of electric dipole transitions in the same ion (Zhang *et al* 2002), retaining only the configurations belonging to the same parity as the ground state in the present work. More precisely, the configurations explicitly introduced into the calculations were $4f^4$, $4f^3 6p$, $4f^3 5f$, $4f^3 6f$, $4f^2 5d^2$, $4f^2 6s^2$, $4f^2 6p^2$ and $4f^2 5d6s$.

In order to reduce as much as possible the differences between calculated and available experimental energy levels in $4f^4$ ground configuration, some radial parameters were adjusted using the well-established least squares optimization procedure of Cowan (1981) in which the observational data were taken from the recent work published by Ding *et al* (2023). More precisely, the 16 experimental energy levels identified by the latter authors as belonging to $4f^4$ were used to fit the average energy (E_{av}), the Slater electrostatic integrals (F^2, F^4, F^6) and the spin-orbit parameter (ζ_{4f}) characterizing this configuration. All the other Slater integrals corresponding to the electrostatic interactions between electrons within the same configuration (F^k, G^k) or belonging to two different configurations (R^k) were scaled down by a factor of 0.85, as suggested by Cowan (1981), while the spin-orbit parameters (ζ_{nl}), computed by the Blume–Watson method, were kept to their *ab initio* values. At the end of the fitting process, the average relative deviation ΔE / E_{Exp} (with $\Delta E = E_{\mathrm{HFR}}$—$E_{\mathrm{Exp}}$) was found to be equal to 0.0040 $\pm$ 0.0035 for all the experimentally known levels in the $4f^4$ configuration. The detailed comparaison between HFR and experimental energy levels is given in table 1.

Table 1. Comparison between the available experimental energy levels within the $4f^4$ ground configuration of Nd II and the calculated values obtained in the present work using the HFR and the MCDHF methods.

				E_{MCDHF}[b]					
Term[a]	J	E_{Exp}[a]	E_{HFR}[b]	SR	VV1	VV2	VV3	VV4	VV4+CV
^{5}I	4	0.000	0	0	0	0	0	0	0
	5	1137.794	1124	1022	1031	1032	1035	1036	1043
	6	2387.544	2368	2178	2188	2188	2193	2194	2212
	7	3714.548	3697	3441	3442	3439	3446	3446	3476
	8	5093.257	5083	4788	4770	4761	4769	4769	4808
^{5}F	2	10 773.962	10 721	14 511	13 152	13 094	13 037	13 029	11 915
	3	11 424.605	11 381	15 113	13 760	13 703	13 649	13 642	12 520
	4	12 181.327	12 123	15 856	14 492	14 427	14 372	14 364	13 250
	5	13 210.278	13 146	16 794	15 444	15 381	15 328	15 321	14 208
^{3}K2	6	14 064.277	14 065	16 639	16 012	15 646	15 552	15 526	15 370
	7	15 153.807	15 130	17 725	17 131	16 759	16 670	16 645	16 464
	8	16 459.136	16 368	18 982	18 401	18 030	17 944	17 920	17 733
^{5}G	3	15 349.601	15 289	21 121	19 022	18 768	18 649	18 623	17 178
	4	16 831.344	16 928	22 423	20 368	20 143	20 058	20 037	18 498
	5	18 313.004	18 321	23 717	21 697	21 490	21 424	21 406	19 850
^{3}H4	5	16 622.337	16 621	21 485	19 290	17 164	18 766	18 726	18 127

[a] Spectroscopic designations and energies from Ding *et al* (2023).
[b] This work.

2.2. *Fully relativistic MCDHF calculations*

The second theoretical method used was the fully relativistic MCDHF approach described by Grant (2007) and Froese Fischer *et al* (2016) using the latest version of the General Relativistic Atomic Structure Program (GRASP), namely GRASP2018 (Froese Fischer *et al* 2019). Since we were only interested in forbidden transitions within the $4f^4$ ground configuration, only the latter was used in a single reference (SR) where all the orbitals, from 1 s to 4f, were optimized on the ground state. Different valence-valence (VV) models of increasing complexity were then built by considering single and double (SD) electron excitations from the 4f orbital to different active sets $\{nl, n'l', n`l', \ldots\}$ where $nl, n'l', n`l', \ldots$ represent the maximum values of the principal (n) and azimuthal (l) quantum numbers of the excited orbitals. More precisely, four VV models were developed with the {5s,5p,5d,5f,5g}, {6s,6p,6d,6f,6g}, {7s,7p,7d,7f,6g} and {8s,8p,8d,8f,6g} active sets, giving rise to the VV1, VV2, VV3 and VV4 models, respectively. In each of these models, only the additional orbitals were optimized, the other ones being maintained frozen at their previously obtained values. As the VV4 model was found to present good convergence of the results (for the energy levels and the forbidden transition rates within the $4f^4$ configuration) obtained in the different successive VV approaches, it is from this VV4 model that a core-valence (CV) model was constructed. In the latter, CV correlation was considered using the relativistic configuration interaction approach in which single electron excitations from the 5 s and 5p core orbitals were permitted to the whole active set. Unlike 5 s and 5p, note that the 4d orbital was not involved in the CV correlation because the $4f^4$ ground configuration of Nd III is such that the 4f orbital is strongly embedded inside the 5 s and 5p orbitals (because of the well-known collapse of the 4f orbital in lanthanide ions) and sits well outside of the 4d orbital, which therefore plays a less important role in the correlation. Furthermore, the opening of the 4d orbital would result in a number of several million configuration state functions (CSFs) whose influence would be very weak on the final results. Finally, it is worth mentioning that a core-core (CC) model was tested (with double excitation from 5 s and 5p orbitals) and it was found that it did not improve the results, the calculated energy levels being slightly further from the experimental values than with the VV4+CV model. The latter was then retained for the final MCDHF calculations, in which a total of 1388 687 CSFs were involved, when limiting the calculations to total angular momentum quantum numbers ranging from $J = 1$ to $J = 10$.

The comparison between the calculated energy levels deduced from the different MCDHF models and the experimentally established values in the $4f^4$ ground configuration of Nd III is reported in table 2. As can be seen from this table, the agreement between the theoretical and experimental results improves with the complexity of the MCDHF model used, the mean relative deviation $\Delta E/E_{\mathrm{Exp}}$ (with $\Delta E = E_{\mathrm{MCDHF}}—E_{\mathrm{Exp}}$) being found to be equal to 0.1815 ± 0.1757, 0.1101 ± 0.1224, 0.0925 ± 0.1185, 0.0959 ± 0.1146, 0.0950 ± 0.1141 and 0.0491 ± 0.0749 for SR, VV1, VV2, VV3, VV4 and VV4+CV models, respectively. As expected, this clearly shows that CV correlation makes it possible to significantly reduce the differences between calculated and observed levels in the case of a heavy ion like Nd III. It is therefore the VV4+CV approach which was adopted for the final MCDHF calculations of transition rates and, even if the experimental energy structure was well reproduced with this model,

the M1 and (E2) transition probabilities were nevertheless corrected using wavelengths deduced from the experimental energy levels observed by Ding *et al* (2023) within the $4f^4$ configuration.

3. Transition probabilities

The transition probabilities of [Nd III] lines computed in the present work using the HFR and the MCDHF (VV4+CV) methods are reported in table 2. All possible M1 and (E2) transitions involving the experimentally known energy levels within the $4f^4$ ground configuration are listed in this table. The Ritz wavelengths (in vacuum) were deduced from the experimental levels obtained by Ding *et al* (2023). A total of 78 forbidden lines was obtained by considering the 16 experimental levels identified by the latter authors as belonging to the $4f^4$ configuration. When looking at table 2, we note that the vast majority of the most intense lines (with *gA*-values of the order of 10^{-1} to 10^{+1} s^{-1}) have a main component of M1 type, the purely E2 transitions appearing systematically much weaker with *gA*-values typically ranging from 10^{-11} to 10^{-3} s^{-1}.

We also note that the HFR and MCDHF transition probabilities show good agreement with each other with an average deviation of about 50% for the whole set of 78 lines listed in table 2. However, it should be emphasized that this deviation is greatly reduced to 35% if we only consider the transitions with *gA*-values larger than 10^{-1} s^{-1} and even reduced down to 25% for the most intense lines with *gA*-values larger than 1 s^{-1}. Such a comparison is illustrated in figure 1 where the HFR transition probabilities are plotted against the MCDHF ones for all [Nd III] lines considered in the present work. Let us also add that to our knowledge, no radiative rate has been published to date for forbidden lines in Nd III, the results obtained in our study are therefore the first available for these transitions.

4. Astrophysical implications

From the new atomic data obtained in our work, it was possible to deduce some astrophysical implications, in particular with regard to the analysis of kilonovae spectra. A first interesting point was to check whether certain assumptions made concerning the presence of [Nd III] lines in kilonovae spectra are verified by our calculations. More particularly, in a recent paper, Gillanders *et al* (2023) investigated which r-process species were able to explain features observed in T_0+29 day *JWST* emission spectrum of GRB 23 0307A. To do so, these authors provided a shortlist of forbidden transitions that were coincident with the two emission features appearing at ∼2.1 μm and ∼4.4 μm. Among those transitions, chosen to fit into the fairly broad profiles of these observed features, namely between 1.94 and 2.35 μm for the first one and between 4.18 and 4.55 μm for the second one, the [Nd III] line at 41 884 Å was presented as one of the candidate forbidden transitions contributing to the 4.4 μm emission feature based on the argument that neodymium is expected to be one of the most abundant lanthanide elements synthesised (Goriely *et al* 2011, 2013, 2015, Bauswein *et al* 2013, Gillanders *et al* 2022) and on the fact that this particular transition has an upper level of low excitation energy making it possible to have a high relative population. However, given the extremely low transition probability obtained in the present work for this line using both theoretical approaches, i.e. $gA_{\rm HFR} = 6.53 \times 10^{-8}$ s^{-1} and $gA_{\rm MCDHF} = 3.87 \times 10^{-8}$ s^{-1}, it seems very unlikely that the latter contributes to the observed spectral feature.

On the other hand, when we examine table 2, we notice that a fairly large number of [Nd III] lines have a relatively high transition probability. So, for example, if we limit ourselves to the wavelength region covered by the *Near Infrared Spectrograph* on board the *JWST*, i.e. 0.6–5.3 μm, we find 21 lines with gA_{HFR}-values ranging from 10^{-1} to 10^{+1} s^{-1}. None of these transitions were cited in previous studies as potential contributors to the features observed in the spectra of late-phase kilonovae. The main reason is that these lines all involve at least one level that does not appear in the NIST atomic database (Kramida *et al* 2024), exclusively used in previous studies, but involve brand new energy levels that have recently been measured experimentally (Ding *et al* 2023), the latter study listing levels belonging to the lowest ^{5}I, ^{5}F, ^{3}K2, ^{5}G and ^{3}H4 multiplets of the $4f^4$ ground configuration while only the five ^{5}I levels are given in the NIST compilation.

Among the 21 strongest Nd III forbidden lines mentioned above, it is important to note that only eight have an upper level whose energy is below the first levels of the opposite parity, starting with $4f^35d\ ^5L_6$ at 15 158.154 cm^{-1}, according to Ding *et al* (2023). More precisely, the most intense [Nd III] lines of table 2 within the 0.6–5.3 μm range and involving both $4f^4$ levels below the opposite parity are those located at 6514.827, 7036.403, 7736.056, 7833.146, 8209.286, 8564.039, 8741.825 and 21 854.871 Å. The last of these lines is particularly interesting since it could contribute to the feature observed at ∼2.1 μm on the *JWST* emission spectrum of GRB 23 0307A at T_0+29 days. This M1 transition meets the selection criteria adopted by Gillanders *et al* (2023), namely a relatively high transition probability, with $gA_{HFR} = 3.18 \times 10^{-1}$ s^{-1} and an upper level energy below 3 eV.

Table 2. Transition probabilities (gA) for [Nd III] lines calculated in the present work using HFR and MCDHF methods.

λ_{vac}[a]	Transition	gA (HFR)[b]	gA (MCDHF)[b]	Rel. Diff.[c]	Type[d]
5460.601	$^5I_4$–$^5G_5$	1.13(−1)	8.25(−2)	0.31	M1
5822.345	$^5I_5$–$^5G_5$	3.00(+0)	1.84(+0)	0.48	M1
5941.296	$^5I_4$–$^5G_4$	4.63(+0)	2.56(+0)	0.58	M1
6016.001	$^5I_4$–$^3H_5$	1.39(−1)	1.60(−1)	−0.14	M1
6279.253	$^5I_6$–$^5G_5$	8.44(+0)	5.31(+0)	0.46	M1
6372.045	$^5I_5$–$^5G_4$	4.80(+0)	2.73(+0)	0.55	M1+E2
6458.053	$^5I_5$–$^3H_5$	4.50(+0)	4.15(+0)	0.08	M1
6514.827	$^5I_4$–$^5G_3$	1.91(−1)	9.41(−2)	0.68	M1+E2
6850.039	$^5I_7$–$^5G_5$	2.69(−1)	1.67(−1)	0.47	E2
6923.386	$^5I_6$–$^5G_4$	2.50(−1)	1.43(−1)	0.54	E2
7025.041	$^5I_6$–$^3H_5$	8.52(+0)	8.34(+0)	0.02	M1
7036.403	$^5I_5$–$^5G_3$	1.77(−1)	1.11(−1)	0.46	E2
7106.516	$^5I_6$–$^3K_8$	1.37(−5)	4.55(−6)	1.00	E2
7110.213	$^5I_4$–$^3K_6$	5.84(−4)	2.39(−4)	0.84	E2
7134.697	$^5I_5$–$^3K_7$	1.39(−4)	5.83(−5)	0.82	E2
7569.863	$^5I_4$–$^5F_5$	2.82(−3)	1.58(−3)	0.56	M1
7736.056	$^5I_5$–$^3K_6$	9.20(+0)	6.52(+0)	0.34	M1
7747.260	$^5I_7$–$^3H_5$	9.30(−2)	3.82(−2)	0.84	E2
7833.146	$^5I_6$–$^3K_7$	1.27(+1)	9.09(+0)	0.33	M1
7846.468	$^5I_7$–$^3K_8$	9.81(+0)	7.22(+0)	0.30	M1
8209.286	$^5I_4$–$^5F_4$	2.63(−1)	1.03(−1)	0.87	M1
8283.299	$^5I_5$–$^5F_5$	9.96(−2)	4.69(−2)	0.72	M1
8564.039	$^5I_6$–$^3K_6$	4.40(+0)	3.15(+0)	0.33	M1
8741.825	$^5I_7$–$^3K_7$	1.19(+1)	8.59(+0)	0.32	M1
8753.038	$^5I_4$–$^5F_3$	3.90(−3)	1.49(−3)	0.89	M1
8798.264	$^5I_8$–$^3K_8$	2.26(+1)	1.66(+1)	0.31	M1
9055.073	$^5I_5$–$^5F_4$	9.61(−2)	3.81(−2)	0.86	M1
9239.809	$^5I_6$–$^5F_5$	1.17(−1)	5.73(−2)	0.69	M1
9281.637	$^5I_4$–$^5F_2$	6.26(−5)	7.14(−6)	1.59	E2
9662.089	$^5I_7$–$^3K_6$	9.42(−2)	6.93(−2)	0.30	M1
9721.186	$^5I_5$–$^5F_3$	2.56(−7)	3.19(−6)	−1.70	E2
9939.814	$^5I_8$–$^3K_7$	1.27(−1)	9.70(−2)	0.27	M1
10 210.559	$^5I_6$–$^5F_4$	1.59(−4)	7.47(−5)	0.72	E2
10 531.049	$^5I_7$–$^5F_5$	2.31(−4)	1.19(−4)	0.64	E2
11 147.004	$^5I_8$–$^3K_6$	4.91(−9)	1.15(−8)	−0.80	E2
14 517.161	$^5F_3$–$^5G_5$	1.47(−3)	9.85(−4)	0.40	E2
16 308.752	$^5F_4$–$^5G_5$	1.76(−2)	6.03(−3)	0.98	M1+E2
16 508.782	$^5F_2$–$^5G_4$	1.02(−3)	5.90(−4)	0.53	E2
18 495.437	$^5F_3$–$^5G_4$	1.76(−3)	1.12(−2)	−1.46	M1+E2
19 239.160	$^5F_3$–$^3H_5$	3.55(−4)	1.51(−4)	0.81	E2
19 597.368	$^5F_5$–$^5G_5$	3.30(−1)	7.66(−2)	1.25	M1
21 505.298	$^5F_4$–$^5G_4$	1.51(−1)	8.98(−3)	1.78	M1
21 854.871	$^5F_2$–$^5G_3$	3.18(−1)	1.51(−1)	0.71	M1
22 517.400	$^5F_4$–$^3H_5$	3.66(−3)	1.63(−2)	−1.27	M1+E2
23 536.462	$^3K_6$–$^5G_5$	3.00(−4)	3.19(−5)	1.62	M1
25 477.733	$^5F_3$–$^5G_3$	1.34(−1)	6.63(−2)	0.68	M1
27 616.177	$^5F_5$–$^5G_4$	2.11(−2)	1.29(−2)	0.48	M1
29 307.817	$^5F_5$–$^3H_5$	7.49(−1)	4.91(−1)	0.42	M1
31 562.927	$^5F_4$–$^5G_3$	9.48(−2)	4.83(−2)	0.65	M1
31 653.613	$^3K_7$–$^5G_5$	5.29(−6)	4.77(−6)	0.10	E2
33 744.988	$^5G_3$–$^5G_5$	8.83(−7)	1.65(−7)	1.37	E2
36 139.349	$^3K_6$–$^5G_4$	2.25(−6)	1.57(−6)	0.36	E2
36 958.835	$^5I_6$–$^5I_8$	1.02(−7)	5.92(−8)	0.53	E2
38 808.516	$^5I_5$–$^5I_7$	1.30(−7)	7.68(−8)	0.51	E2
39 092.125	$^3K_6$–$^3H_5$	2.57(−5)	9.41(−6)	0.93	M1
41 756.112	$^3K_6$–$^3K_8$	2.38(−8)	8.86(−9)	0.91	E2
41 884.045	$^5I_4$–$^5I_6$	6.53(−8)	3.87(−8)	0.51	E2

(Continued.)

Table 2. (Continued.)

λ_{vac}[a]	Transition	gA (HFR)[b]	gA (MCDHF)[b]	Rel. Diff.[c]	Type[d]
46 743.760	$^5F_5$–$^5G_3$	2.97(−8)	1.76(−8)	0.51	E2
51 452.795	$^5F_5$–$^3K_7$	5.83(−9)	3.53(−9)	0.49	E2
53 108.155	$^5F_4$–$^3K_6$	1.16(−8)	4.90(−9)	0.81	E2
56 001.295	$^5F_3$–$^5F_5$	2.04(−7)	8.77(−8)	0.80	E2
59 148.253	$^3H_5$–$^5G_5$	4.42(−1)	4.31(−1)	0.03	M1
67 488.087	$^5G_3$–$^5G_4$	1.49(+0)	1.41(+0)	0.06	M1
67 491.867	$^5G_4$–$^5G_5$	1.36(+0)	1.74(+0)	−0.25	M1
68 095.306	$^3K_7$–$^3H_5$	4.88(−8)	9.57(−8)	−0.65	E2
71 054.773	$^5F_2$–$^5F_4$	9.11(−8)	3.63(−8)	0.86	E2
72 531.622	$^5I_7$–$^5I_8$	1.81(+0)	1.78(+0)	0.02	M1
73 357.723	$^5I_6$–$^5I_7$	2.37(+0)	2.35(+0)	0.01	M1
76 609.039	$^3K_7$–$^3K_8$	7.17(−1)	8.55(−1)	−0.18	M1
78 570.890	$^5G_3$–$^3H_5$	4.65(−11)	6.53(−11)	−0.34	E2
80 016.003	$^5I_5$–$^5I_6$	1.93(+0)	1.95(+0)	−0.01	M1
87 889.372	$^5I_4$–$^5I_5$	9.56(−1)	9.89(−1)	−0.03	M1
91 782.695	$^3K_6$–$^3K_7$	4.31(−1)	4.79(−1)	−0.11	M1
97 186.358	$^5F_4$–$^5I_6$	3.68(−1)	3.76(−1)	−0.02	M1
117 096.156	$^5F_5$–$^3K_6$	8.42(−11)	5.54(−11)	0.41	M1+E2
132 148.927	$^5F_3$–$^5F_4$	1.92(−1)	2.09(−1)	−0.08	M1
153 694.115	$^5F_2$–$^5F_3$	1.32(−1)	1.28(−1)	0.03	M1
478 452.875	$^3H_5$–$^5G_4$	1.47(−3)	3.91(−4)	1.16	M1

[a] Vacuum wavelengths, in Å, deduced from the experimental energy levels (Ding *et al* 2023).
[b] Sum of M1 and E2 gA-values, in s^{-1}. A(B) stands for A × 10^B.
[c] Relative difference evaluated by $\Delta gA/\overline{gA}$ where $\Delta gA = gA$(HFR) – gA(MCDHF) and $\overline{gA} = (gA(\text{HFR}) + gA(\text{MCDHF}))/2$.
[d] Contributions larger than 10%.

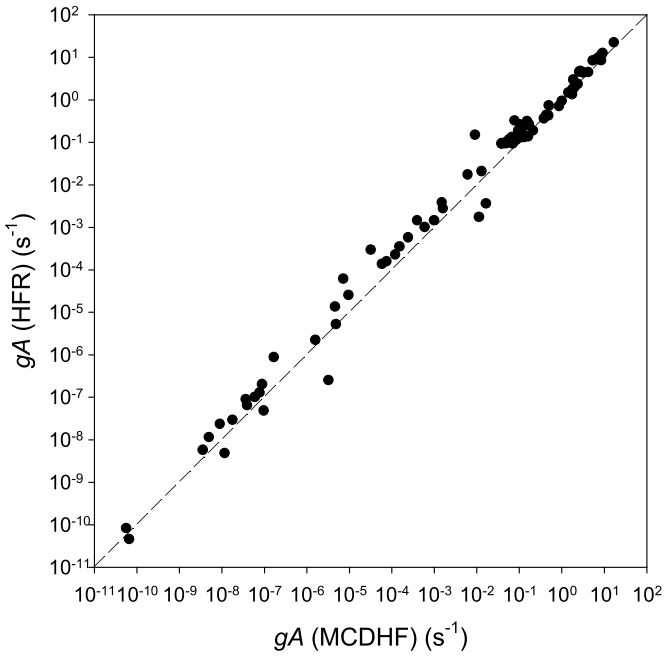

Figure 1. Comparison between transition probabilities computed for forbidden lines in Nd III using HFR and MCDHF methods.

5. Conclusions

A new set of transition probabilities for M1 and E2 lines within the $4f^4$ ground configuration of Nd III was obtained for the first time in the present work from two independent computational methods, namely the HFR and the fully relativistic Dirac-Hartree–Fock (MCDHF) methods. The overall agreement between the results deduced from these two approaches was found to be good with a relative deviation not exceeding 25% for the most intense lines. From these new atomic data, a list of some [Nd III] transitions that could be expected to be detectable on the astrophysical spectra recorded by the

JWST Near Infrared Spectrograph (0.6–5.3 μm) was established, among which a line appearing at 21 854.871 Å presents a fairly large gA-value to be a candidate forbidden line contributing to the observed feature located at $\sim$2.1 μm on the emission spectrum of GRB 23 0307A at T_0+29 days (Gillanders *et al* 2023).

Data availability statement

All data that support the findings of this study are included within the article (and any supplementary files).

Acknowledgment

P P and P Q are, respectively, Research Associate and Research Director of the Belgian Fund for Scientific Research F.R.S—FNRS. This project has received funding from the FWO and F.R.S—FNRS under the Excellence of Science (EOS) programme (Numbers 0.0228.18 and 0.0004.22). Part of the atomic calculations were made with computational resources provided by the Consortium des Equipements de Calcul Intensif (CECI), funded by the F.R.S—FNRS Under Grant No. 2.5020.11 and by the Walloon Region of Belgium.

ORCID iDs

P Palmeri https://orcid.org/0000-0002-4372-6798
P Quinet https://orcid.org/0000-0002-3937-2640

References

Abbott B P, Abbott R, Abbott T D, Acernese F and Ackley K 2017 *Phys. Rev. Lett.* **119** 161101
Allehabi S O, Dzuba V A and Flambaum V V 2021 *Phys. Rev.* A **104** 053109
Arnold K J, Kaewuam R, Roy A, Paez E, Wang S and Barett M D 2016 *Phys. Rev.* A **94** 052512
Bar-Shalom A, Klapich M and Oreg J 2001 *J. Quantum Spectrosc. Radiat. Transfer* **71** 169
Bauswein A, Goriely S and Janka H T 2013 *Astrophys. J.* **773** 78
Beck D R and O'Malley S M 2010 *J. Phys. B: At. Mol. Opt. Phys.* **43** 215003
Beloy K, Sherman J A, Lemke N D, Hinkley N, Oates C W and Ludlow A D 2007 *Phys. Rev.* A **86** 051404
Biémont E, Ellmann A, Lundin P, Mannervik S, Norlin L O, Palmeri P, Quinet P, Rostohar D, Royen P and Schef P 2007 *Eur. Phys. J.* D **41** 211
Biémont E and Quinet P 1998 *Phys. Rev. Lett.* **81** 3345
Bowers C J, Budker D, Freedman S J, Gwinner G, Stalnaker J E and DeMille D 1999 *Phys. Rev.* A **59** 3513
Chaudhuri R K, Freed K F, Chattopadhyay S and Mahapatra U S 2012 *Europhys. Lett.* **98** 23002
Cowan R D 1981 *The Theory of Atomic Structure and Spectra* (California University Press)
Derkatch A, Ilyinsky L, Mannervik S, Norlin L O, Rostohar D, Royen P, Schef P and Biémont E 2002 *Phys. Rev.* A **65** 062508
Ding M, Pickering J C, Ryabtsev A N, Kononov E Y and Ryabchikova T 2023 arXiv:2307.09282
Dzuba V A and Derevianko A 2010 *J. Phys. B: At. Mol. Opt. Phys.* **43** 074011
Dzuba V A and Flambaun V V 2011 *Phys. Rev.* A **83** 052513
Dzuba V A and Flambaun V V 2012 *Phys. Rev.* A **85** 012515
Dzuba V A, Flambaun V V and Schiller S 2018 *Phys. Rev.* A **98** 022501
Fawcett B C and Wilson M 1991 *Atom. Data Nucl. Data Tables* **47** 241
Froese Fischer C, Gaigalas G, Jönsson P and Biéron J 2019 *Comput. Phys. Commun.* **237** 184
Froese Fischer C, Godefroid M, Brage T, Jönsson P and Gaigalas G 2016 *J. Phys. B: At. Mol. Opt. Phys.* **49** 182004
Gerz C, Roths J, Vedel F and Werth G 1988 *Z. Phys.* D **8** 235
Gillanders J H, McCann M, Sim A S, Smartt J S and Ballance C P 2021 *Mon. Not. R. Astron. Soc.* **506** 3560
Gillanders J H, Smartt S J, Sim S A, Bauswein A and Goriely S 2022 *Mon. Not. R. Astron. Soc.* **515** 631
Gillanders J H, Troja E, Fryer C L, Ristic M, O'Connor B 2023 arXiv:2308.00633
Goriely S, Bauswein A and Janka H T 2011 *Astrophys. J.* **738** L32
Goriely S, Bauswein A, Just O, Pllumbi E and Janka H T 2015 *Mon. Not. R. Atron. Soc.* **452** 3894
Goriely S, Sida J L, Lemaître J F, Panebianco S, Dubray N, Hilaire S, Bauswein A and Janka H T 2013 *Phys. Rev. Lett.* **111** 242502
Gossel G H, Dzuba V A and Flambaum V V 2013 *Phys. Rev.* A **88** 034501
Grant I P 2007 *Relativistic Quantum Theory of Atoms and Molecules. Theory and Computations* (Springer)
Hotokezaka K, Tanaka M, Kato D and Gaigalas G 2021 *Mon. Not. R. Astron. Soc.* **506** 5863
Jönsson P, Gaigalas G, Bieroń J, Froese F C and Grant I P 2013 *Comput. Phys. Commun.* **184** 2197
Karaçoban B and Özdemir L 2011 *Acta Phys. Pol.* A **119** 342
Kasen D, Metzger B, Barnes J, Quataert E and Ramirez-Ruiz E 2017 *Nature* **551** 80
Kasliwal M M *et al* 2022 *Mon. Not. R. Astron. Soc.* **510** L7
Kolachevsky N, Akimov A, Tolstikhina I, Chebakov K, Sokolov A, Rodionov P, Kanorski S and Sorokin V 2007 *Appl. Phys.* B **89** 589
Kozlov M G, Dzuba V A and Flambaum V V 2019 *Phys. Rev.* A **99** 012516
Kramida A, Ralchenko Y and Reader J 2024 NIST atomic spectra database (available at: https://physics.nist.gov/asd)
Lange R, Peshkov A A, Huntemann N, Tamm C, Surzhykov A and Peik E 2021 *Phys. Rev. Lett.* **127** 213001
Levan A, Gompertz B P, Salafia O S, Bulla M and Burns E 2023 arXiv:2307.02098
Li H, Kuang X Y and Yeung Y Y 2014 *J. Phys. B: At. Mol. Opt. Phys.* **47** 145002
Li H, Kuang X Y and Yeung Y Y 2016 *J. Lumin.* **170** 380
Migdalek J and Baylis W E 1991 *J. Phys. B: At. Mol. Opt. Phys.* **24** L99
Mishra A P and Balasubramanian T K 2001 *J. Quant. Spectrosc. Radiat. Transfer* **69** 769
Nandy D K and Sahoo B K 2014 *Phys. Rev.* A **90** 050503
Paez E, Arnold K J, Hajiyev E, Porsev S G, Dzuba V A, Safronova U I, Safronova M S and Barett M D 2016 *Phys. Rev.* A **93** 042112
Pian E *et al* 2017 *Nature* **551** 67
Pian E 2023 *Universe* **9** 105
Roberts B M, Dzuba V A and Flambaum V V 2013 *Phys. Rev.* A **88** 012510
Roberts B M, Dzuba V A and Flambaum V V 2014a *Phys. Rev.* A **89** 042509
Roberts B M, Dzuba V A and Flambaum V V 2014b *Phys. Rev.* A **89** 012502
Roberts B M, Dzuba V A and Flambaum V V 2015 *Annu. Rev. Nucl. Part. Sci.* **65** 63
Roberts M, Taylor P, Barwood G P, Gill P, Klein A and Rowley W R C 1997 *Phys. Rev. Lett.* **78** 1876

Rostohar D, Andersson K, Derkatch A, Hartman H, Mannervik S, Norlin L O, Royen P, Schmitt A and Tordoir X 2001 *Phys. Scr.* **64** 237
Rostohar D, Derkatch A, Hartman H, Norlin L O, Royen P, Shef P and Mannervik S 2003 *Hyperf. Interact.* **146–147** 151
Safronova M S, Porsev S G, Sanner C and Ye J 2018 *Phys. Rev. Lett.* **120** 173001
Safronova U I and Safronova M S 2009 *Phys. Rev.* A **79** 032511
Safronova U I and Safronova M S 2014 *Phys. Rev.* A **89** 052515
Safronova U I, Safronova M S and Johnson W R 2016 *Phys. Rev.* A **94** 032506
Sahoo B K and Das B P 2011 *Phys. Rev.* A **84** 010502
Siegel D M 2022 *Nat. Rev. Phys.* **4** 306
Smartt S J *et al* 2017 *Nature* **551** 75
Stalnaker J E, Budker D, DeMille D P, Freedman S J and Yashchuk V V 2002 *Phys. Rev.* A **66** 031403
Sukachev D, Fedorov D, Tolstikhina I, Tregubov D, Kalganova E, Vishnyakova G, Golovizin A, Kolachevsky N, Khabarova K and Sorokin V 2016 *Phys. Rev.* A **94** 022512
Tan T R, Edmunds C L, Milne A R, Biercuk M J and Hempel C 2021 *Phys. Rev.* A **104** L010802
Tsigutkin K, Dounas-Frazer D, Family A, Stalnaker J E, Yashchuk V V and Budker D 2009 *Phys. Rev. Lett.* **103** 071601
Tsigutkin K, Dounas-Frazer D, Family A, Stalnaker J E, Yashchuk V V and Budker D 2010 *Phys. Rev.* A **81** 032114
Xu C Y *et al* 2014 *Phys. Rev. Lett.* **113** 033003
Yu N and Maleki L 2000 *Phys. Rev.* A **61** 022507
Zhang Z G, Svanberg S, Palmeri P, Quinet P and Biémont E 2002 *Astron. Astrophys.* **385** 724